Hydrothermal synthesis of delafossite $CuScO_2$ hexagonal plates as electrocatalyst for the alkaline oxygen evolution reaction

Yanwen Deng,[a] Dehua Xiong,*[,a] Han Gao,[a] Jie Wu,[a] Santosh Kumar Verma,[b] Baoshun Liu,[a] and Xiujian Zhao*[,a]

[a] State Key Laboratory of Silicate Materials for Architectures, Wuhan University of Technology, Wuhan 430070, P. R. China

* Corresponding author Email: xiongdehua2010@gmail.com (Dehua Xiong), opluse@whut.edu.cn (Xiujian Zhao)

[b] Department of Chemistry and Chemical Engineering, Yulin University, Yulin 719000, P. R. China

Experimental details:

Materials synthesis

All chemicals used in the experiments were purchased from Sinopharm Chemical Reagent Co., Ltd with analytical grade and used as received without further purification. $CuScO_2$ were prepared according to a procedure reported in our previous works (*J. Mater. Chem.*, 2012, 22, 24760-24768; *New J. Chem.*, 2016, 40, 6498-6504; *Inorg. Chem. Front.,* 2018, 5, 183-188.). Typically, 15 mmol $Cu(NO_3)_2 \cdot 3H_2O$ and 15 mmol $Sc(NO_3)_3 \cdot xH_2O$ were dissolved sequentially in 70 ml deionized water at room temperature, 0.50 ml ethylene glycol and 5.00 g NaOH was added to the above solution for preparing the hydrothermal precursor. The mixture was stirred for 30 minutes at room temperature until a homogeneous suspension formed, and then the solution was loaded into a 100 mL Teflon-lined autoclave reactor which was kept at 240 ºC in an oven for 24 hours. Subsequently, the autoclave reactor was naturally cooled down to room temperature. The as-obtained precipitates were collected and washed with diluted ammonia aqueous solution, deionized water and ethanol for 3 times to remove any byproduct impurities. Finally, the as-obtained $CuScO_2$ powders were dried at 60 °C for 12 hours for further characterization.

Structural characterization

The morphology, microstructure, and chemical composition of $CuScO_2$ powders were examined by field-emission scanning electron microscopy (FESEM, FEG Quanta 450) equipped with energy-dispersive X-ray

spectroscopy (EDX). The crystalline structure of $CuScO_2$ powders was studied by X-ray diffractometry (XRD, PANalytical X'Pert PRO) using Cu K_α radiation (λ = 1.540598 Å) and a PIXcel detector. The surface chemical states of $CuScO_2$ powders were analyzed by X-ray photoelectron spectroscopy (XPS, Thermo Escalab 250Xi), and the C (1s) line (at 284.80 eV) corresponding to the surface adventitious carbon (C−C line bond) has been used as the reference binding energy. The thermal stability of $CuScO_2$ powders was investigated by a differential scanning calorimetry-thermogravimetry analyzer (DSC-TG, Diamond TG/DTA, Perkin-Elmer Instruments) from 25 °C to 1000 °C at a heating rate of 10 °C/min under air atmosphere.

Electrochemical measurements

The electrocatalytic activity towards oxygen evolution reaction was evaluated by cyclic voltammetry (CV) scan in a three-electrode configuration in 1.0 M KOH (pH = 13.5) using a CS2350H electrochemical workstation (Wuhan Corrtest Instruments Corp., China). A platinum wire and a saturated calomel electrode (SCE) were used as the counter and reference electrodes, respectively. The Ni@$CuScO_2$ working electrodes were fabricated as follows: $CuScO_2$ powders were dispersed in a mixture of 500 μL water, 480 μL isopropanol and 20 μL Nafion (5 wt%, Sigma), and cast onto a piece of nickel foam (the working area is 10×10 mm^2). The $CuScO_2$ loading mass was kept as 0.15, 0.30, and 0.45 mg cm^{-2}, these working electrodes were denoted as Ni@$CuScO_2$-0.15, Ni@$CuScO_2$-0.30, and Ni@$CuScO_2$-0.45. Cyclic voltammetric (CV)

scans were recorded between 1.00 and 1.90 V *vs.* reversible hydrogen electrode (RHE) at a scan rate of 5 mV s^{-1}.

All current density values are normalized with respect to the geometrical surface area of the working electrode. All CV curves presented in this work are *iR*-corrected (85%). The correction was done according to the following equation:

$$E_c = E_m - iR_s \quad (1)$$

where E_c is the *iR*-corrected potential, E_m experimentally measured potential, and R_s the equivalent series resistance extracted from the electrochemical impedance spectroscopy measurements. Unless otherwise specified, all potentials are reported versus reversible hydrogen electrode (RHE) by converting the potentials measured *vs.* SCE according to the following formula:

$$E\ (RHE) = E\ (SCE) + 0.241 + 0.059\ pH \quad (2)$$

Supplementary figures:

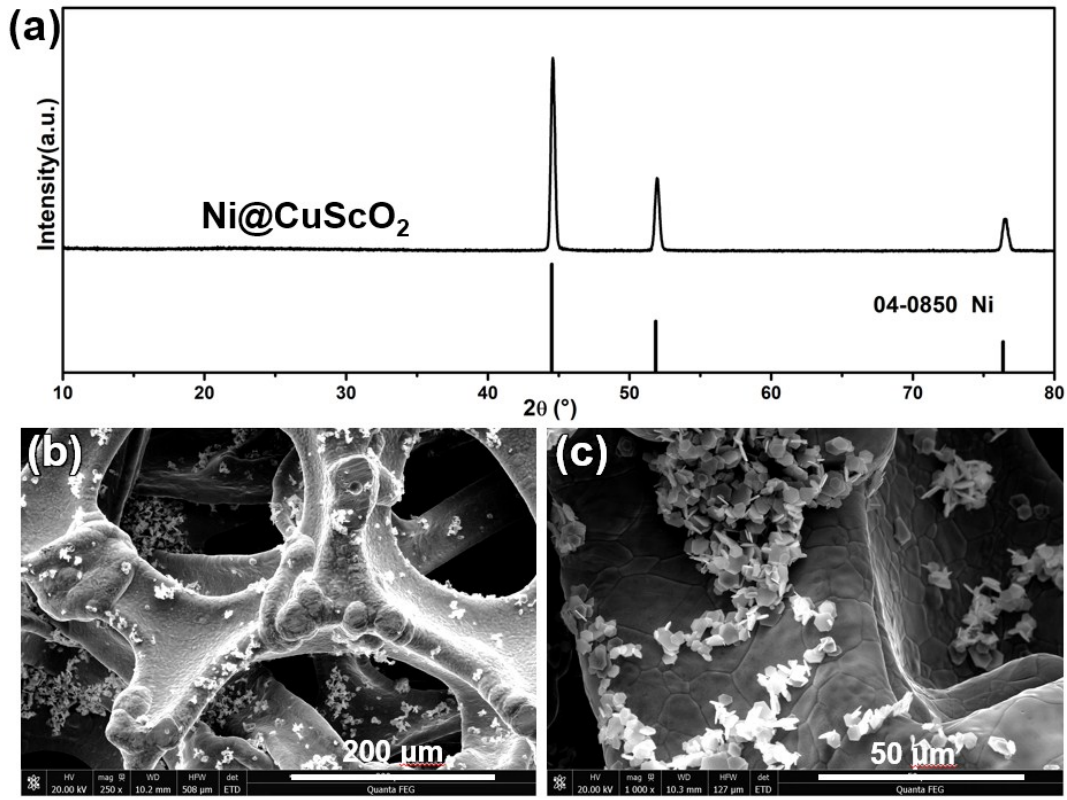

Fig. S1. XRD patterns (a) and SEM images (b, c) of Ni@$CuScO_2$-0.30 working electrodes.

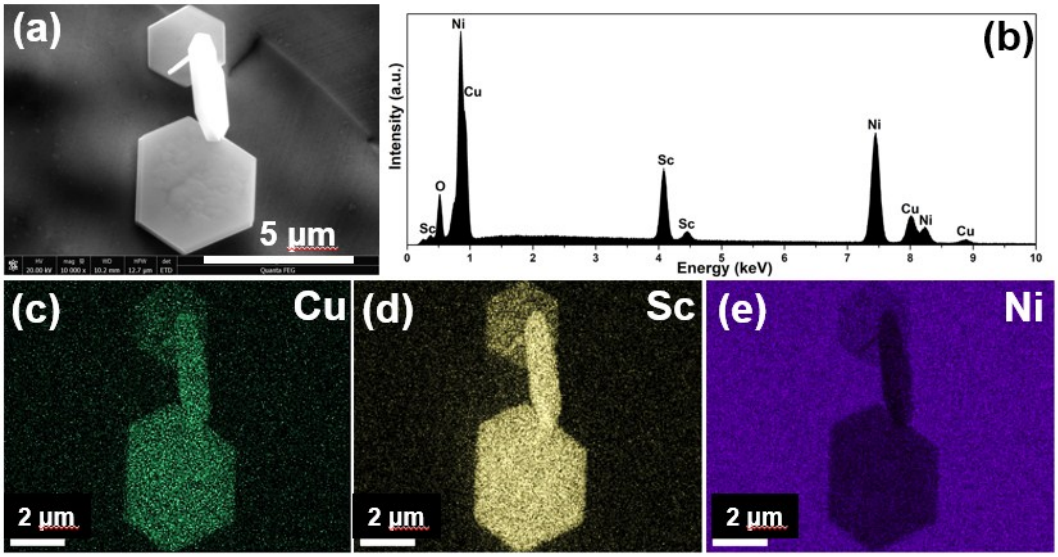

Fig. S2. SEM image (a), EDX spectrum (b) and elemental maps (c, Cu; d, Sc; e, Ni) of Ni@$CuScO_2$-0.30 working electrodes.

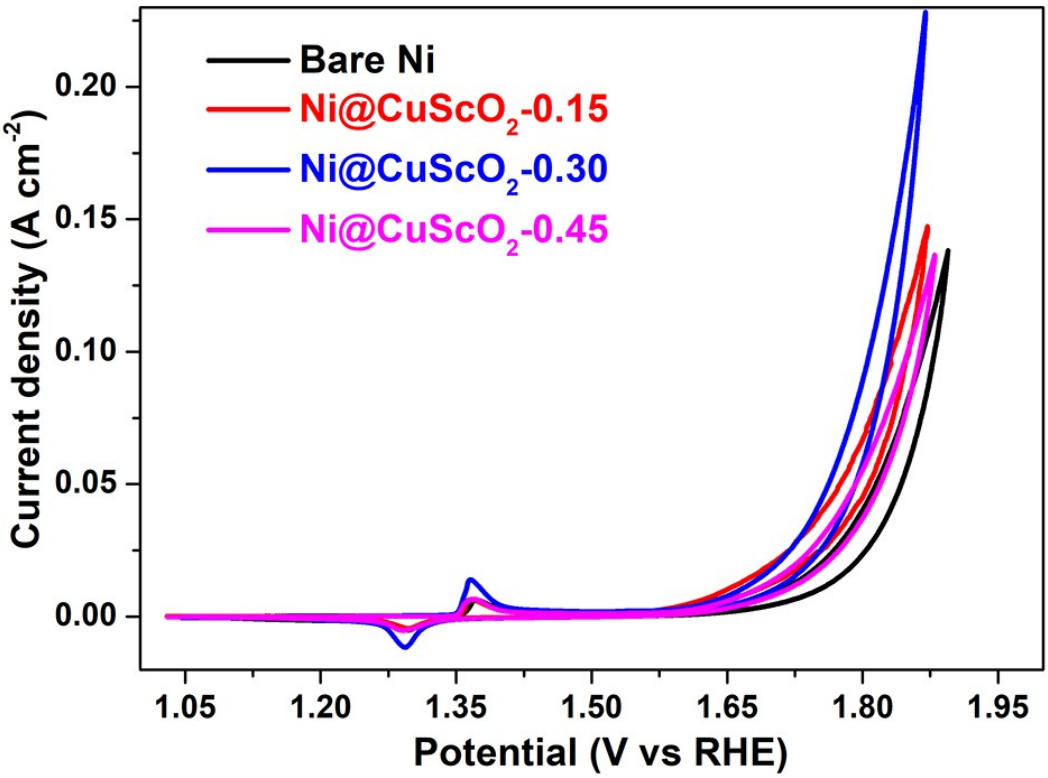

Fig. S3. CV curves recorded at a scan rate of 5 mV s^{-1} in the potential range of 1.00 to 1.90 V vs RHE, and the loading mass of Ni@$CuScO_2$ working electrodes were 0.15, 0.30, and 0.45 mg cm^{-2}.

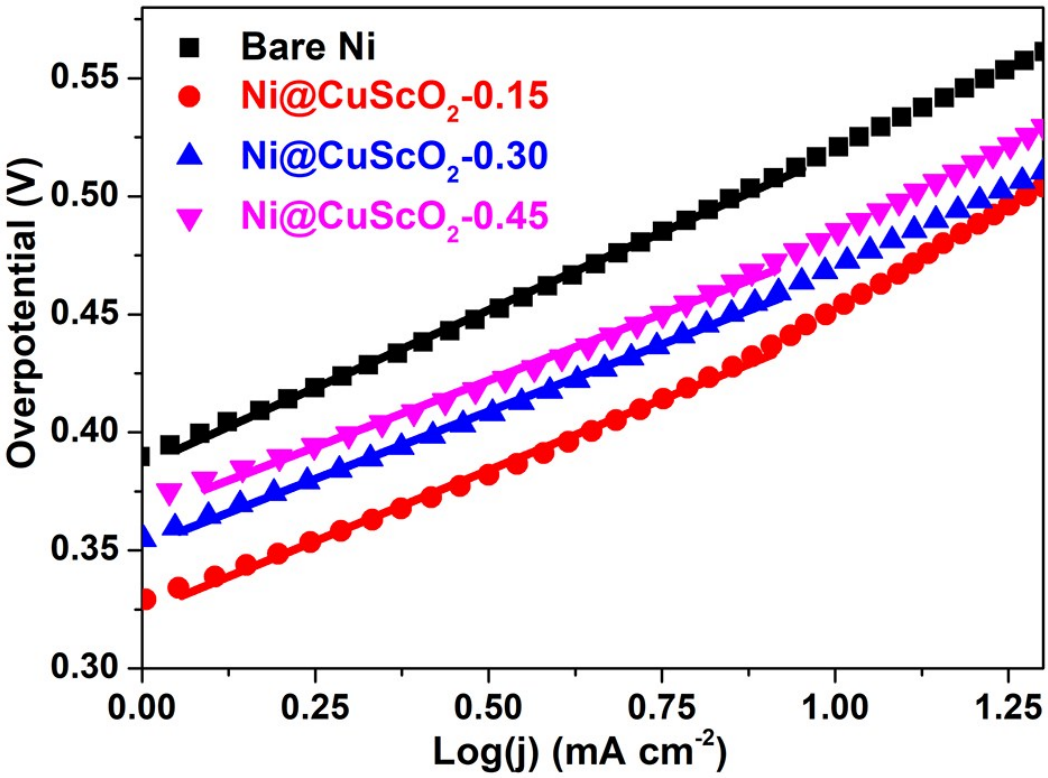

Fig. S4. Tafel plots of the bare Ni and Ni@$CuScO_2$ working electrodes.

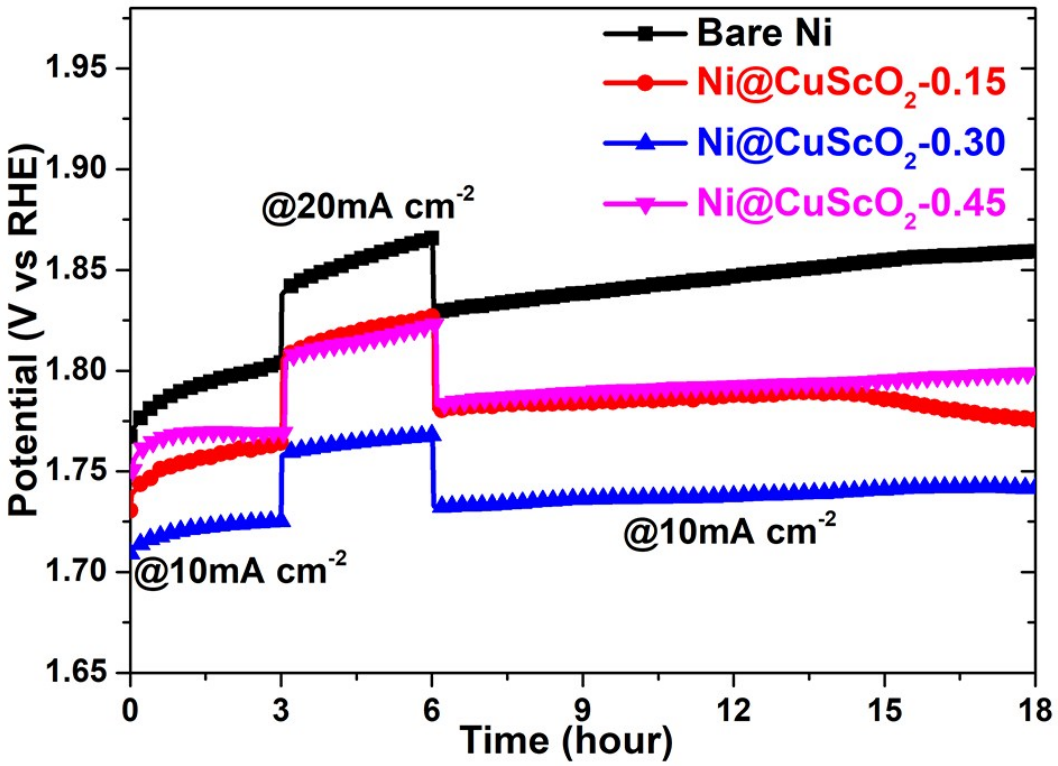

Fig. S5. Chronopotentiometric curves of bare Ni and Ni@$CuScO_2$ working electrodes measured for 18 hours.

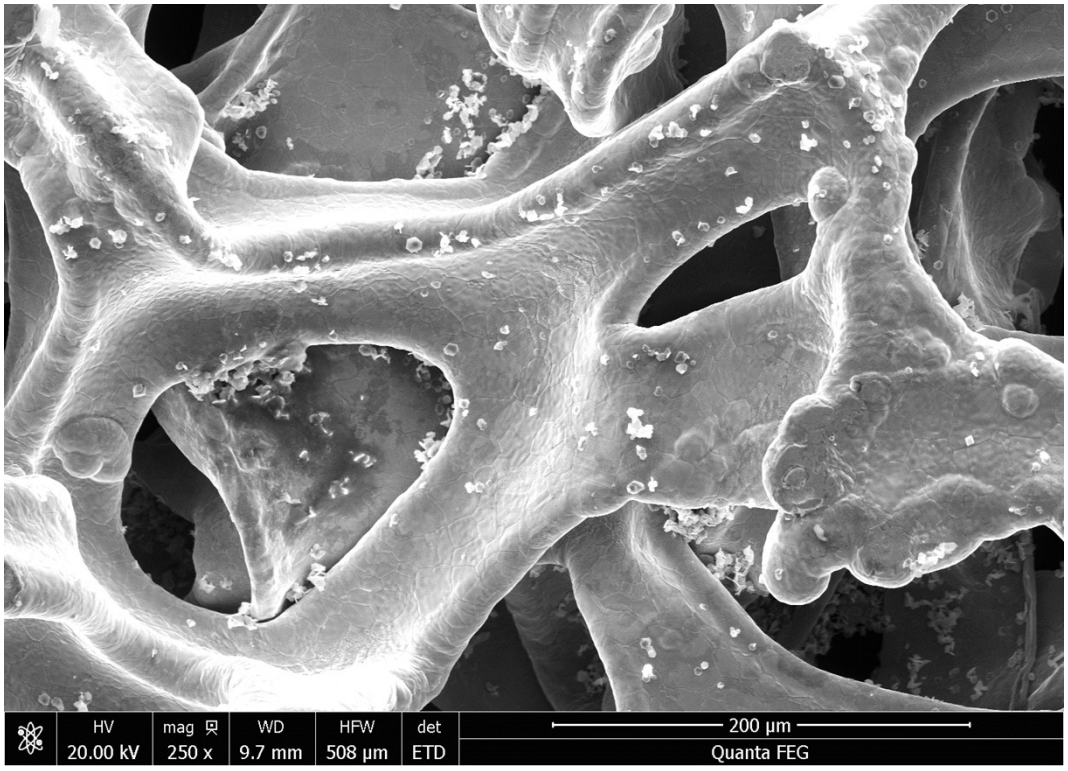

Fig. S6. SEM image of Ni@$CuScO_2$-0.30 working electrodes after long-term stability test for 18 hours under OER conditions.

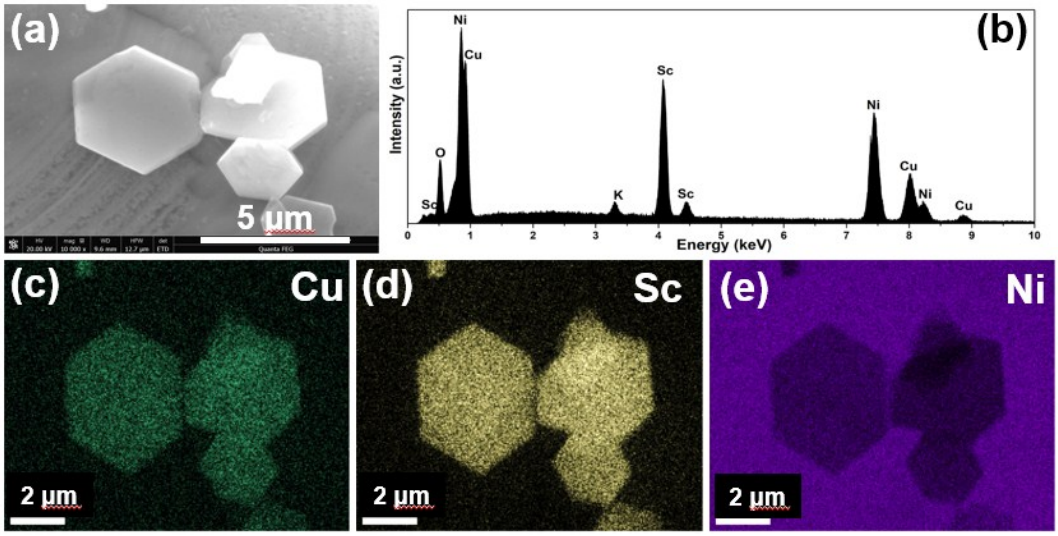

Fig. S7. SEM image (a), EDX spectrum (b) and elemental maps (c, Cu; d, Sc; e, Ni) of Ni@$CuScO_2$-0.30 working electrodes after long-term stability test for 18 hours under OER conditions.

Supplementary Table:

Table S1. The OER activity of Ni@$CuScO_2$ electrodes in comparison to that of other ternary metal oxides based OER catalysts recently reported in the literatures.

Catalysts	Electrolyte	Loading mass (mg cm^{-2})	Tafel slope (mV dec^{-1})	J_{geo} (current density in mA cm^{-2} @overpotential in mV)	Reference
Ni@$CuScO_2$	1.0 M KOH	0	132	10@η=520 20@η=570	This work
		0.30	114	10@η=470 20@η=510	
5%-La-excess $LaNiO_3$	0.1 M KOH	-	~70	0.042@η=400	*Nano Lett.* 2017, 17, 3126-3132.
5%-Ni-excess $LaNiO_3$			~70	0.121@η=400	
$LaCoO_3$-bulk	0.1 M KOH	0.25	102	10@η=620	*Nat. Commun.,* 2016, 7, 11510.
$LaCoO_3$- 60 nm			78	10@η=550	
$LaCoO_3$- 80 nm			69	10@η=490	
$LaCoO_3$- 200 nm			89	10@η=540	
$LaFeO_3$	0.1 M KOH	0.464	77	10@η=510	*Chem. Mater.* 2016, 28, 1691-1697.
$La_{0.95}FeO_{3-\delta}$			48	1@η=320 10@η=410	
$SrCoO_3$	0.1 M KOH	-	145	0.7@η=350	*Mater. Horiz.,* 2015, 2, 495-501.
$SrSc_{0.025}Nb_{0.025}Co_{0.95}O_{3-\delta}$			~70	10@η=350	
$LiCoO_2$ 20–100 nm	1.0 M NaOH	0.32	48 ± 3	10@η=430±14	*Energy Environ. Sci.,* 2016, 9, 184-192.
$LiCoO_2$ 50–150 nm		1.20	49 ± 3	10@η=430 ± 8	
$CuRhO_2$	1.0 M KOH	20 μmol/cm^2	-	10@η=420	*J. Phys. Chem. C* 2015, 119, 6495-6501.
$CuCrO_2$			-	5@η=710	
$CuCoO_2$			-	10@η=430	
$CuFeO_2$			-	5@η=670	
$CuCoO_2$	1.0 M KOH	0.30	93	1@η=390 10@η=440	*Inorg. Chem. Front.,* 2018,5, 183-188.
$CuMnO_2$	1.0 M	0.05	-	12.3@ 2.0 V	*Journal of The*

	KOH			vs. Ag/AgCl 10@ 1.69 V vs. Ag/AgCl	*Electrochemical Society,* 2019,166 (6) H233-H242.
$NiCo_2O_4$	1.0 M KOH	-	75	10@η=460	*Appl. Surf. Sci.,* 2017, 416, 371-378.
$Fe_{0.5}Ni_{0.5}Co_2O_4$			27	10@η=350	
$ZnCo_2O_4$	0.1 M KOH	0.051	38.5	20@η=420	*J. Mater. Chem.* A, 2016, 4, 10014-10022.
Ni-Mn-O nanomeshs	0.1 M KOH	1±0.2	41	10@η=372	*Electrochimica Acta,* 2017, 245, 32-40.
Ni-Mn-O nanoparticles			59	10@η=275	
$CoFe_2O_4$ thin films	1.0 M NaOH	-	54.2	10@η=490	*Electrochem. Commun.,* 2018, 87, 1-4.